Curve Reconstruction in Inverse Problems: From Divergence-Measure Vector Fields to Density Lebesgue Measures

Anéva Doliciane Tsafack, Laure Blanc-Féraud, Gilles Aubert

Curve Reconstruction in Inverse Problems: From Divergence-Measure Vector Fields to Density Lebesgue Measures

Anéva Doliciane Tsafack[1], Laure Blanc-Féraud[1], and Gilles Aubert[2]

[1]Université Côte d'Azur, CNRS, I3S, INRIA, Morpheme project, France
(Aneva-Doliciane.Tsafack@univ-cotedazur.fr, blancf@i3s.unice.fr)
[2]Université Côte d'Azur, CNRS, LJAD, France (Gilles.AUBERT@univ-cotedazur.fr)

Abstract

We present a novel variational framework for curve reconstruction in inverse problems, formulated through vector field optimization. The problem is defined in a space of vector-valued measures absolutely continuous with respect to the Lebesgue measure, with Sobolev-type densities. Within this setting, we establish an equivalence, in terms of minimizers, between the proposed functional and a previously defined one within the space of divergence-measure fields. This formulation enables the use of standard convex optimization algorithms for numerical implementation. Furthermore, we propose an acquisition model specifically adapted to blurred curves in microscopy images, leading to promising numerical results.

Keywords: inverse problems, curve reconstruction, divergence-measure fields, vector field, imaging.

1. Introduction

In ill-posed inverse problems, finding a regularizer that promotes curve structures is of great interest in many image applications, including the super-resolution of filament structures in fluorescence microscopy images.

Recent work by Laville et al. [9] introduced the optimization functional CROC (Curves Represented on Charges):

$$\arg\min_{m\in\mathcal{V}(\mathcal{X})} \underbrace{\frac{1}{2}\left\|y-\Phi(m)\right\|_{\mathcal{H}}^{2}}_{\text{data term}} + \lambda \underbrace{\left\|m\right\|_{\mathcal{V}(\mathcal{X})}}_{\text{regularizer}}, \tag{CROC}$$

where y denotes the observed data, $\Phi : \mathcal{V}(\mathcal{X}) \to \mathcal{H}$ is a linear and continuous forward operator, $\mathcal{H}$ is the observation space (either $L^2(\mathcal{X})$ or $\mathbb{R}^N$ for discrete measurements), and $\lambda > 0$ is a regularization parameter. The key result shown in [9] is that this functional admits a solution that is a linear combination of measures supported on curves, making

it suitable for performing curve reconstruction. Specifically, for a discrete measurement $y \in \mathbb{R}^N$, $N \in \mathbb{N}^*$, a solution is given by:

$$\sum_{i=1}^{N} a_i \mu_{\gamma_i},$$

where $a_i \in \mathbb{R}$ and μ_{γ_i} is a vector-valued measure supported on a Lipschitz parametrized curve γ_i, defined in the distributional sense by

$$\langle \mu_{\gamma_i}, g \rangle = \int_0^1 g(\gamma_i(t)) \cdot \dot{\gamma}_i(t) \, \mathrm{d}t, \qquad \forall \, g \in \mathcal{C}_0(\mathcal{X}, \mathbb{R})^2.$$

This structural property follows from the choice of regularizer, which is defined by the norm

$$\|\cdot\|_{\mathcal{V}(\mathcal{X})} = \|\cdot\|_{\mathcal{M}(\mathcal{X})^2} + \|\mathrm{div}(\cdot)\|_{\mathcal{M}(\mathcal{X})},$$

on the space of divergence-measure fields

$$\mathcal{V}(\mathcal{X}) = \left\{ m \in \mathcal{M}(\mathcal{X})^2 : \mathrm{div}(m) \in \mathcal{M}(\mathcal{X}) \right\},$$

where $\mathcal{X}$ is a locally compact Hausdorff topological space, and $\mathcal{M}(\mathcal{X})^2$ and $\mathcal{M}(\mathcal{X})$ denote the spaces of 2-dimensional and 1-dimensional finite signed Radon measures on $\mathcal{X}$, respectively. Elements of this space $\mathcal{V}(\mathcal{X})$ can be decomposed into curves, as established in [13, 2, 12].

While the theoretical framework is well-established, the challenge lies in developing an algorithm to effectively reconstruct these curve-based solutions. In [8], the authors introduced a Curve Sliding Frank-Wolfe algorithm, which is an extension of the Sliding Frank-Wolfe algorithm (a conditional gradient-based algorithm) developed in [6], to solve the CROC functional. The key step in this algorithm involves addressing the certificate of the functional by solving an optimization problem in the space of curves, formulated as:

$$\arg\max_{\gamma} \left(\frac{|\langle \mu_\gamma, \eta \rangle|}{\|\mu_\gamma\|_{\mathcal{V}(\mathcal{X})}} \right),$$

where η, the certificate, is defined as:

$$\eta = \frac{1}{\lambda} \Phi^*(\Phi m - y),$$

with $\Phi^* : \mathcal{H} \to \mathcal{C}_0(\mathcal{X}, \mathbb{R})^2$ being the adjoint operator of Φ, and $m \in \mathcal{V}(\mathcal{X})$ a solution of the CROC functional. This optimization problem in the space of curves is challenging. Furthermore, the algorithm incorporates a non-convex step over the set of curves and their amplitudes.

Since optimizing the CROC functional directly in $\mathcal{V}(\mathcal{X})$ is challenging and no straightforward algorithm is currently available, this work proposes a relaxation of (CROC) in

the space of measures absolutely continuous with respect to the Lebesgue measure. In this space, the density functions can be discretized, enabling the use of standard convex optimization algorithms for implementation.

1.1 Contributions

We introduce a space of vector-valued Lebesgue measures whose densities are vector-valued functions in L^1 with divergence also in L^1:

$$\mathcal{W}(\mathcal{X}) = \left\{ f \, \mathrm{d}x \mid f \in L^1(\mathcal{X})^2,\ \mathrm{div}(f) \in L^1(\mathcal{X}) \right\},$$

and prove that $\mathcal{W}(\mathcal{X})$ is dense in $\mathcal{V}(\mathcal{X})$ with respect to the weak-* topology on the measures and the local weak-* topology on their divergences (Section 3).

Next, in Section 4, we formulate the original CROC functional in the space $\mathcal{W}(\mathcal{X})$, leading to the definition of the relaxed functional $\mathrm{CROC}_{\mathrm{R}}$:

$$\operatorname*{arg\,min}_{f\,\mathrm{d}x \in \mathcal{W}(\mathcal{X})} D_\lambda(f) \overset{\text{def.}}{=} \frac{1}{2} \|y - \Phi(f\,\mathrm{d}x)\|_{\mathcal{H}}^2 + \lambda \left(\|f\|_{L^1(\mathcal{X},\mathbb{R}^2)} + \|\mathrm{div}(f)\|_{L^1(\mathcal{X},\mathbb{R})} \right), \quad (\mathrm{CROC_R})$$

and establish the equivalence of their infima (Theorem 4.3):

$$\inf_{m \in \mathcal{V}(\mathcal{X})} T_\lambda(m) = \inf_{m \in \mathcal{W}(\mathcal{X})} D_\lambda(m).$$

This result ensures that every minimizing sequence of $\mathrm{CROC}_{\mathrm{R}}$ converges to a solution of the original CROC functional (Proposition 4.4). This finding provides a theoretical foundation for the practical use of $\mathrm{CROC}_{\mathrm{R}}$.

Finally, in Section 5, we present numerical experiments to illustrate the proposed approach and highlight its promising performance for the problem of curve reconstruction in blurry and noisy fluorescence microscopy images, using simulated examples.

2. Preliminary Concepts and Notations

This section provides a brief overview of the mathematical concepts relevant to our study; further details can be found in [1, 11, 4].

Notation 2.1. *We denote by $\mathcal{X}$ an open bounded subset of $\mathbb{R}^2$.*

Definition 2.2. *We denote by $\mathcal{C}_c(\mathcal{X}, \mathbb{R})$ the space of continuous functions from $\mathcal{X}$ to $\mathbb{R}$ with compact support. The space $\mathcal{C}_0(\mathcal{X}, \mathbb{R})$, called the space of vanishing (or evanescent) continuous functions, consists of continuous functions $f : \mathcal{X} \to \mathbb{R}$ that vanish at infinity, i.e.,*

$$\forall \epsilon > 0,\ \exists K_\epsilon \subset \mathcal{X} \text{ compact},\ \forall x \in \mathcal{X} \setminus K_\epsilon,\ |f(x)| \leq \epsilon.$$

This space is equipped with the supremum norm $\|\cdot\|_\infty$, defined as:

$$\forall f \in \mathcal{C}_0(\mathcal{X}, \mathbb{R}), \quad \|f\|_\infty := \sup_{x \in \mathcal{X}} |f(x)|.$$

Note that the closure of $\mathcal{C}_c(\mathcal{X}, \mathbb{R})$ under the supremum norm $\|\cdot\|_\infty$ is precisely $\mathcal{C}_0(\mathcal{X}, \mathbb{R})$.

Let $n \in \mathbb{N}^*$. We denote by $\mathcal{C}_0(\mathcal{X}, \mathbb{R})^n$ the space of continuous vector-valued functions $\mathbf{f} = (f_1, \dots, f_n) : \mathcal{X} \to \mathbb{R}^n$ such that $f_i \in \mathcal{C}_0(\mathcal{X}, \mathbb{R})$ for all i. This space is equipped with the supremum norm defined by

$$\|\mathbf{f}\|_\infty := \max_{i=1,\dots,n} \|f_i\|_\infty = \max_{i=1,\dots,n} \left(\sup_{x \in \mathcal{X}} |f_i(x)| \right).$$

Definition 2.3 (Topological dual space)**.** *Let E be a normed vector space. The* dual space *of E, denoted E^*, is the set of all continuous linear functionals from E into $\mathbb{R}$ or $\mathbb{C}$. The* weak-* topology *on E^* is defined as the coarsest topology for which all evaluation maps*

$$f \in E^* \longmapsto f(x) \in \mathbb{R} \text{ or } \mathbb{C}, \quad x \in E,$$

are continuous. A sequence $(f_n)_{n \in \mathbb{N}}$ in E^* is said to weak-* converge *to $f \in E^*$, denoted by $f_n \overset{*}{\rightharpoonup} f$, if*

$$\forall x \in E, \quad f_n(x) \xrightarrow[n \to \infty]{} f(x) \quad \textit{(pointwise convergence).}$$

Definition 2.4 (Finite Radon measure)**.** *Let $n \in \mathbb{N}^*$. We denote by $\mathcal{M}(\mathcal{X})^n$ the space of n-dimensional vector-valued finite Radon measures, that is, the topological dual of $\mathcal{C}_0(\mathcal{X}, \mathbb{R})^n$ equipped with the supremum norm.*

The duality pairing between $m \in \mathcal{M}(\mathcal{X})^n$ and $\varphi \in \mathcal{C}_0(\mathcal{X}, \mathbb{R})^n$ is defined as

$$\langle m, \varphi \rangle := \int_{\mathcal{X}} \varphi \, \mathrm{d}m = \sum_{i=1}^{n} \int_{\mathcal{X}} \varphi_i \, \mathrm{d}m_i.$$

The norm associated with the strong topology on $\mathcal{M}(\mathcal{X})^n$, called the total variation norm*, is defined by*

$$\|m\|_{\mathrm{TV}} := \sup \left\{ \langle m, \varphi \rangle \mid \varphi \in \mathcal{C}_0(\mathcal{X}, \mathbb{R})^n, \ \|\varphi\|_\infty \leq 1 \right\}, \quad \forall m \in \mathcal{M}(\mathcal{X})^n.$$

Definition 2.5 (Space of distributions)**.** *The space of distributions on $\mathcal{X}$, denoted $\mathcal{D}'(\mathcal{X})$, is the topological dual of the space of smooth functions with compact support on $\mathcal{X}$, $\mathcal{C}_c^\infty(\mathcal{X}, \mathbb{R})$. Its closure in the sup-norm satisfies*

$$\overline{\mathcal{C}_c^\infty(\mathcal{X}, \mathbb{R})}^{\|\cdot\|_\infty} = \mathcal{C}_0(\mathcal{X}, \mathbb{R}),$$

so that $\mathcal{M}(\mathcal{X})$ is a subset of $\mathcal{D}'(\mathcal{X})$.

Definition 2.6 (Divergence of a vector-valued measure)**.** *Let $m \in \mathcal{M}(\mathcal{X})^2$ be a vector-*

valued Radon measure on $\mathcal{X}$. The divergence *of m, denoted by* $\operatorname{div}(m)$*, is defined in the sense of distributions by*

$$\langle \operatorname{div}(m), \varphi \rangle := -\int_{\mathcal{X}} \nabla\varphi \cdot \mathrm{d}m, \quad \forall\, \varphi \in C_c^\infty(\mathcal{X}, \mathbb{R}).$$

Definition 2.7 (Total variation measure)**.** *Let m be an n-dimensional vector-valued Radon measure on $\mathcal{X}$, and let $\mathcal{B}(\mathcal{X})$ denote the Borel σ-algebra on $\mathcal{X}$. For every open set $A \subset \mathcal{X}$, define*

$$|m|(A) := \sup\left\{ \langle m, \varphi \rangle \mid \varphi \in \mathcal{C}_0(A, \mathbb{R})^n,\ \|\varphi\|_\infty \leq 1 \right\}.$$

The measure $|m|$ extends to all Borel sets $E \in \mathcal{B}(\mathcal{X})$ by outer regularity:

$$|m|(E) := \inf\left\{ |m|(A) \mid E \subset A,\ A \text{ open in } \mathcal{X} \right\}.$$

Moreover, the total variation norm of m coincides with the total mass of its total variation measure:

$$\|m\|_{\mathrm{TV}} = |m|(\mathcal{X}).$$

Definition 2.8 (Local weak-* and weak-* convergence of vector-valued Radon measures)**.** *Let $n \in \mathbb{N}^*$. A sequence $(\mu_h)_h \subset \mathcal{M}(\mathcal{X})^n$* local weak-* converges *to $\mu \in \mathcal{M}(\mathcal{X})^n$, denoted $\mu_h \overset{*}{\rightharpoonup} \mu$ locally, if*

$$\lim_{h\to\infty} \int_{\mathcal{X}} u \,\mathrm{d}\mu_h = \int_{\mathcal{X}} u \,\mathrm{d}\mu, \quad \forall u \in C_c(\mathcal{X}, \mathbb{R})^n. \tag{1}$$

If equation (1) holds for all $u \in C_0(\mathcal{X}, \mathbb{R})^n$, then $(\mu_h)_h$ is said to weak-* converge *to μ, denoted $\mu_h \overset{*}{\rightharpoonup} \mu$.*

For $(\mu_h)_h \subset \mathcal{V}(\mathcal{X})$, we say $(\mu_h)_h$ weak-* converges *to $\mu \in \mathcal{V}(\mathcal{X})$ if*

$$\mu_h \overset{*}{\rightharpoonup} \mu \quad \text{in } \mathcal{M}(\mathcal{X})^2, \quad \operatorname{div}(\mu_h) \overset{*}{\rightharpoonup} \operatorname{div}(\mu) \quad \text{in } \mathcal{M}(\mathcal{X}).$$

Proposition 2.9. *The weak*-convergence of a sequence $(\mu_h)_h \subset \mathcal{M}(\mathcal{X})^n$ is equivalent to the local weak*-convergence together with the condition $\sup_h |\mu_h|(\mathcal{X}) < \infty$.*

Definition 2.10 (Standard symmetric mollifier family)**.** *A standard symmetric mollifier family $(\rho_\varepsilon)_{\varepsilon>0}$ on $\mathbb{R}^2$ is a family of functions in $C_c^\infty(\mathbb{R}^2, \mathbb{R})$ such that, for each $\varepsilon > 0$,*

$$\rho_\varepsilon \geq 0, \qquad \operatorname{supp}(\rho_\varepsilon) \subset \overline{B}(0, \varepsilon), \qquad \int_{\mathbb{R}^2} \rho_\varepsilon(x)\,\mathrm{d}x = 1, \qquad \rho_\varepsilon(x) = \rho_\varepsilon(-x).$$

Lemma 2.11. *Let $u \in L^\infty(\mathcal{X})$. Then there exists a sequence $(u_n)_{n\in\mathbb{N}} \subset C_c^\infty(\mathcal{X}, \mathbb{R})$ such that*

$$\|u_n\|_\infty \leq \|u\|_\infty \quad \forall n \in \mathbb{N}, \quad u_n \to u \text{ almost everywhere in } \mathcal{X},$$

and

$$u_n \overset{*}{\rightharpoonup} u \quad \text{in } L^\infty(\mathcal{X}) \text{ under the weak-* topology } \sigma(L^\infty, L^1).$$

We recall this characterization of the L^1-norm, which is a direct consequence of Lemma 2.11.

Remark 2.12 (Dual characterization of the L^1-norm [4])**.** *For any $g \in L^1(\mathcal{X})$,*

$$\sup \left\{ \int_{\mathcal{X}} g\, \varphi \, \mathrm{d}x \;\middle|\; \varphi \in C_c^\infty(\mathcal{X}, \mathbb{R}),\ \|\varphi\|_\infty \leq 1 \right\} = \|g\|_{L^1(\mathcal{X})}.$$

Definition 2.13 (Parametrized curve)**.** *A parametrized curve in $\mathbb{R}^2$ is a continuous map $\gamma : [0,1] \to \mathbb{R}^2$. The parametrized curve γ is said to be* Lipschitz *if γ is a Lipschitz map, and* simple *if γ is injective on $[0,1)$.*

We now turn to the measure-theoretic framework underlying our formulation.

A natural first candidate for approximating vector measures would be vectors of finite linear combinations of Dirac masses. However, although such measures are weak*-dense in $\mathcal{M}(\mathcal{X})^2$ [3], they do not belong to $\mathcal{V}(\mathcal{X})$ [9]. This motivates the introduction, in the following section, of the space $\mathcal{W}(\mathcal{X})$ of vector measures that are absolutely continuous with respect to the Lebesgue measure.

3. The Space $\mathcal{W}$: Definition and Analysis

Definition 3.1. *We denote by $\mathcal{W}(\mathcal{X})$ the space of vector-valued measures on $\mathcal{X} \subseteq \mathbb{R}^2$ that are absolutely continuous with respect to the Lebesgue measure, whose densities and divergences (in the distributional sense) belong to L^1. That is,*

$$\mathcal{W}(\mathcal{X}) = \left\{ f \, \mathrm{d}x \;\middle|\; f \in L^1(\mathcal{X})^2,\ \mathrm{div}(f) \in L^1(\mathcal{X}) \right\}.$$

Here, $\mathrm{d}x$ denotes the Lebesgue measure on $\mathbb{R}^2$, with $\mathrm{d}x := \mathrm{d}x_1\, \mathrm{d}x_2$ for $x = (x_1, x_2) \in \mathbb{R}^2$.

Working in $\mathcal{W}(\mathcal{X})$ is convenient for algorithmic purposes, since elements are represented by density functions with divergences, which can be discretized on a grid over $\mathcal{X}$.

Proposition 3.2. *The space $\mathcal{W}(\mathcal{X})$ is a subspace of $\mathcal{V}(\mathcal{X})$. Moreover, for every $f\,dx \in \mathcal{W}(\mathcal{X})$,*

$$\|f\,dx\|_{\mathrm{TV}} = \|f\|_{L^1(\mathcal{X})^2} := \sum_{i=1}^{2} \|f_i\|_{L^1(\mathcal{X})},$$

and

$$\|\,\mathrm{div}(f\,dx)\|_{\mathrm{TV}} = \|(\mathrm{div}\, f)\,dx\|_{\mathrm{TV}} = \|\,\mathrm{div}\, f\|_{L^1(\mathcal{X})}.$$

Proof. The result is a straightforward consequence of the dual characterization of the L^1-norm given in Remark 2.12, the density of $C_c^\infty(\mathcal{X})$ in $C_0(\mathcal{X})$ with respect to the supremum norm, and the Riesz representation theorem, applied to the linear functionals

$$T_f : C_c^\infty(\mathcal{X}, \mathbb{R})^2 \to \mathbb{R}, \qquad T_f(\varphi) := \int_{\mathcal{X}} f \cdot \varphi \, \mathrm{d}x,$$

and

$$S_f : C_c^\infty(\mathcal{X}, \mathbb{R}) \to \mathbb{R}, \qquad S_f(\phi) := \int_{\mathcal{X}} (\operatorname{div} f)\phi \, \mathrm{d}x.$$

Moreover, for every $\phi \in C_c^\infty(\mathcal{X})$,

$$\langle \operatorname{div}(f \, \mathrm{d}x), \phi \rangle = -\int_{\mathcal{X}} f \cdot \nabla \phi \, \mathrm{d}x = \int_{\mathcal{X}} (\operatorname{div} f)\phi \, \mathrm{d}x,$$

so that $\operatorname{div}(f \, \mathrm{d}x) = (\operatorname{div} f) \, \mathrm{d}x$ in the sense of distributions. □

The following density result holds.

Proposition 3.3. *The space $\mathcal{W}(\mathcal{X})$ is dense in $\mathcal{V}(\mathcal{X})$ with respect to the local weak-* topology. Specifically, for every $m \in \mathcal{V}(\mathcal{X})$, there exists a family $(f_\varepsilon \, \mathrm{d}x)_{\varepsilon>0} \subset \mathcal{W}(\mathcal{X})$ such that*

$$f_\varepsilon \, \mathrm{d}x \overset{*}{\rightharpoonup} m \quad \text{in } \mathcal{M}(\mathcal{X})^2, \qquad \operatorname{div}(f_\varepsilon) \, \mathrm{d}x \overset{*}{\rightharpoonup} \operatorname{div}(m) \text{ locally in } \mathcal{M}(\mathcal{X}), \quad \text{as } \varepsilon \to 0.$$

Remark 3.4 (Density result for non-bounded open sets $\Omega \subset \mathbb{R}^2$)**.** *The density result of Proposition 3.3 extends to arbitrary unbounded open sets $\Omega \subset \mathbb{R}^2$.*

The proofs of Proposition 3.3 and remark 3.4 are given in Appendix A.

Remark 3.5. *More generally, for all $p \in \mathbb{N}$, the space $\mathcal{W}^p(\mathcal{X})$, defined by*

$$\mathcal{W}^p(\mathcal{X}) = \left\{ f \, \mathrm{d}x \mid f \in L^p(\mathcal{X})^2, \ \operatorname{div}(f) \in L^p(\mathcal{X}) \right\},$$

is dense in $\mathcal{V}(\mathcal{X})$ for the local weak-topology. The proof is obtained by following the same process as above, since the constructed sequence $(f_\epsilon \mathrm{d}x)_{\epsilon>0}$ also lies in $\mathcal{W}^p(\mathcal{X}) \subset \mathcal{W}(\mathcal{X})$, as $\mathcal{X}$ is a bounded subset of $\mathbb{R}^2$.*

In the following section, we define a relaxation of the CROC functional on $\mathcal{W}(\mathcal{X})$ and provide a proof of its connection with the original CROC functional. This allows to explore new optimization strategies while ensuring consistency with the established functional framework.

4. CROC Relaxation Functional

Before defining the relaxation of the CROC functional in $\mathcal{W}(\mathcal{X})$, we first revisit its definition.

Definition 4.1 (CROC functional)**.** *Let $y \in \mathcal{H} := L^2(\mathcal{X})$ and let $\Phi : \mathcal{V}(\mathcal{X}) \to \mathcal{H}$ be a linear map. The* CROC *(Curves Represented on Charges) functional is defined as:*

$$\underset{m \in \mathcal{V}(\mathcal{X})}{\arg\min} \, T_\lambda(m) \overset{def.}{=} \frac{1}{2} \|y - \Phi(m)\|_{\mathcal{H}}^2 + \lambda \|m\|_{\mathcal{V}(\mathcal{X})},$$

where $m \in \mathcal{V}(\mathcal{X})$, and $\lambda \in \mathbb{R}^+$ is the regularization parameter. The operator $\Phi(m)$ is defined as: $\Phi(m) := \int_{\mathcal{X}} \phi(x)\,\mathrm{d}m(x)$, where $\phi \in L^1(\mathcal{X}, \mathcal{H})$ is the kernel of the operator Φ. Specifically, ϕ is often given by:

$$\forall x \in \mathcal{X}, \quad \phi(x) : \mathcal{X} \to \mathbb{R}, \quad \text{with } \phi(x)(y) = \varphi(x - y),\ \forall y \in \mathcal{X}.$$

For Φ to be well-defined and weak*-to-weak continuous, φ must be in $L^2(\mathcal{X})^2$ and, for any $q \in L^2(\mathcal{X})^2$, $\varphi * q$ must belong to $C_0(\mathcal{X}, \mathbb{R})^2$. Note that $\varphi \in C_0(\mathcal{X}, \mathbb{R})^2$ is a sufficient condition.

Under this setting, the CROC functional admits a minimizer that can be written as a finite linear combination of measures supported on curves lying in $\mathcal{X}$, in the case of discrete acquisitions such as images (see Introduction and [9]).

Definition 4.2 (The $\mathrm{CROC_R}$ functional)**.** *The* CROC *functional in the space $\mathcal{W}(\mathcal{X})$, denoted as* $\mathrm{CROC_R}$*, is given by:*

$$\underset{f\mathrm{d}x \,\in\, \mathcal{W}(\mathcal{X})}{\arg\min}\ D_\lambda(f) \overset{def.}{=} \frac{1}{2}\left\|y - \Phi(f\mathrm{d}x)\right\|_{\mathcal{H}}^2 + \lambda\left(\|f\|_{L^1(\mathcal{X})^2} + \|\mathrm{div}(f)\|_{L^1(\mathcal{X})}\right) \tag{2}$$

The following theorem establishes that the infimum of the CROC functional coincides with the infimum of its relaxed version, $\mathrm{CROC_R}$.

Theorem 4.3 (Infimum Equivalence between CROC and $\mathrm{CROC_R}$)**.**

$$\inf_{m \in \mathcal{V}(\mathcal{X})} T_\lambda(m) = \inf_{m \in \mathcal{W}(\mathcal{X})} D_\lambda(m). \tag{3}$$

The proof of Theorem 4.3 is given in Appendix B.

Proposition 4.4. *Any minimizing sequence for the functional* $\mathrm{CROC_R}$ *in $\mathcal{W}(\mathcal{X})$ has a subsequence that converges to a minimizer of the functional* CROC *in $\mathcal{V}(\mathcal{X})$.*

Proof. Let $(m_n)_n$ be a minimizing sequence for D_λ in $\mathcal{W}(\mathcal{X})$, meaning

$$D_\lambda(m_n) \to \inf_{m \in \mathcal{W}(\mathcal{X})} D_\lambda(m) \quad \text{as} \quad n \to \infty.$$

Since D_λ is coercive, the sequence $(m_n)_n$ is bounded. Thus, we can extract a subsequence (m_{n_k}) that converges to a limit point $\overline{m}$ in $\mathcal{V}(\mathcal{X})$. Since T_λ is lower semicontinuous with respect to the weak-* topology, we have

$$T_\lambda(\overline{m}) \leq \liminf_{k\to\infty} T_\lambda(m_{n_k}) = \liminf_{k\to\infty} D_\lambda(m_{n_k}) = \inf_{m \in \mathcal{W}(\mathcal{X})} D_\lambda(m) = \inf_{m \in \mathcal{V}(\mathcal{X})} T_\lambda(m),$$

where the last equality follows from Theorem 4.3. Hence,

$$T_\lambda(\overline{m}) = \inf_{m \in \mathcal{V}(\mathcal{X})} T_\lambda(m),$$

so that $\overline{m}$ is indeed a minimizer of the CROC functional. In conclusion, every minimizing sequence of $\mathrm{CROC}_{\mathrm{R}}$ has a subsequence that converges to a minimizer of CROC. □

Having presented the functional $\mathrm{CROC}_{\mathrm{R}}$, we now explore it numerically. In the following section, we describe an optimization approach to minimize this functional and illustrate its practical interest in recovering curves from blurred and noisy velocity fields. Furthermore, we show how this framework can be applied to curve reconstruction from blurred and noisy images, as typically encountered in fluorescence microscopy.

5. Numerical Exploration

Before presenting the optimization approach, we first define the acquisition operator Φ, which models the physical measurement process. We begin with the problem of deconvolution and denoising of vector fields.

5.1 Deconvolution of Vector Fields

Consider the problem of reconstructing a vector field from blurred and noisy observations. The acquisition process can be modeled by a linear operator Φ that maps a vector field f to the observation space $\mathcal{H}^2$ (typically $\mathcal{H}^2 = \mathbb{R}^N \times \mathbb{R}^N$ for square image with N pixels) via the associated measure $f\,dx$ in $\mathcal{W}(\mathcal{X})$:

$$\Phi : \mathcal{W}(\mathcal{X}) \to \mathcal{H}^2, \quad f\,dx \mapsto \Phi(f\,dx) = (f_1 * h, f_2 * h),$$

where $f = (f_1, f_2)$, $*$ denotes the convolution operator, and h is a blur kernel and discretization.

Let $y = (y_1, y_2)$ denote the observed vector field components. The problem can then be formulated as:

$$\text{Find } f \text{ such that } y = \Phi(f\mathrm{d}x) + \eta,$$

where η represents additive noise. The associated $\mathrm{CROC}_{\mathrm{R}}$ optimization functional is:

$$\underset{f\,\mathrm{d}x \in \mathcal{W}(\mathcal{X})}{\arg\min} \ \frac{1}{2}\|y_1 - f_1 * h\|_{\mathcal{H}}^2 + \frac{1}{2}\|y_2 - f_2 * h\|_{\mathcal{H}}^2 + \lambda\|f\|_{L^1(\mathcal{X})^2} + \lambda\|\operatorname{div}(f)\|_{L^1(\mathcal{X})}. \quad (4)$$

For the numerical implementation, the spatial domain $\mathcal{X}$ is discretized into a grid of $N = N_1 \times N_2$ pixels, denoted by $(P_{i,j})_{1\le i\le N_1,\, 1\le j\le N_2}$, where N_1 and N_2 denote the number of pixels along the x_1- and x_2-directions, respectively.

We represent the unknown vector field by its values on the pixels of the grid. More precisely, to each pixel $P_{i,j}$ we associate a vector $w_{i,j} \in \mathbb{R}^2$, and we identify the discrete unknown with the array

$$w_N = (w_{i,j})_{1\le i\le N_1,\, 1\le j\le N_2} \in (\mathbb{R}^2)^{N_1\times N_2}.$$

The discrete divergence is defined by

$$(\mathrm{div}_N\, w_N)_{i,j} = \begin{cases} w^1_{i,j} - w^1_{i-1,j}, & 1 < i < N_1, \\ w^1_{i,j}, & i = 1, \\ -\, w^1_{i-1,j}, & i = N_1, \end{cases} + \begin{cases} w^2_{i,j} - w^2_{i,j-1}, & 1 < j < N_2, \\ w^2_{i,j}, & j = 1, \\ -\, w^2_{i,j-1}, & j = N_2. \end{cases}$$

This scheme corresponds to the negative adjoint of the discrete gradient and is described in [5]. The forward operator is discretized accordingly and is denoted by Φ_N, so that the discrete functional reads

$$D_{\lambda,N}(w_N) = \frac{1}{2}\,\|y - \Phi_N w_N\|^2_{\mathbb{R}^N} + \lambda \left(\sum_{i=1}^{N_1} \sum_{j=1}^{N_2} \big(|w^1_{i,j}| + |w^2_{i,j}|\big) + \sum_{i=1}^{N_1} \sum_{j=1}^{N_2} |(\mathrm{div}_N\, w_N)_{i,j}| \right).$$

To make the discrete functional differentiable, we replace the absolute value function by a smooth approximation defined as

$$x \mapsto \sqrt{x^2 + \epsilon} - \sqrt{\epsilon},$$

where $\epsilon > 0$ is a small positive constant controlling the degree of smoothing. The resulting functional is convex and continuously differentiable, enabling the use of gradient-based optimization algorithms. For our simulations, we used the L-BFGS (Limited-memory Broyden–Fletcher–Goldfarb–Shanno) algorithm [10], implemented in PyTorch. It is a quasi-Newton method that approximates the inverse Hessian using a history of successive gradients, enabling fast convergence.

Illustration

To illustrate the behavior of the proposed functional, we consider the problem of recovering curves from blurred and noisy discrete velocity vector fields, provided as pixel-based observations in the space $\mathcal{H}^2 \simeq \mathbb{R}^{2N}$, with each vector field component an N-dimensional vector. The synthetic data are generated from predefined curves $\{\gamma_i\}_{i=1}^K$ as follows: for each curve γ_i, we define a vector field $\mathbf{v}^i(x) = \dot{\gamma}_i(t)$ if $x = \gamma_i(t)$ for some $t \in [0,1]$, and $\mathbf{v}^i(x) = 0$ elsewhere. The full velocity field is then obtained by summing over all curves:

$$\mathbf{v}(x) = \sum_{i=1}^{K} \mathbf{v}^i(x).$$

Then each component of $\mathbf{v}$ is blurred with a Gaussian kernel and corrupted with additive Gaussian noise to produce the observations. In all experiments below, we use a Gaussian blur kernel with standard deviation $\sigma_{\mathrm{psf}} = 3 \times 10^{-2}$, expressed in normalized spatial coordinates over $\mathcal{X} = [0,1] \times [0,1]$, and additive Gaussian noise with standard deviation $\sigma_{\mathrm{noise}} = 1 \times 10^{-2}$.

In the first experiment, presented in Figure 1, the vector field is reconstructed by solving the $\mathrm{CROC}_{\mathrm{R}}$ functional using the algorithm described above. Once the reconstructed velocity field $\hat{f}$ is obtained, the corresponding integral curves are computed by solving the differential equation

$$\frac{d\gamma(t)}{dt} = \hat{f}(\gamma(t)), \quad \gamma(0) = x_0, \tag{5}$$

for a set of initial points $x_0 \in \mathcal{X}$, one for each curve to be recovered.

Although $\hat{f}$ is discrete, it is interpolated over the domain $\mathcal{X}$ before solving the differential equation using a fourth-order Runge–Kutta scheme. A finer discretization of f during the optimization improves the quality of the interpolation.

The success of the integration strongly depends on the choice of initial points. To this end, we exploit the reconstructed vector field, which separates the different curves effectively.

Specifically, we compute the magnitude of $\hat{f}$, apply a slight threshold to obtain a skeleton, and then detect its endpoints using the morphological operator **binary hit-or-miss transform** [7, 14], implemented in `scipy.ndimage.binary_hit_or_miss`. This operator identifies pixels that match a specific local pattern defined by the structuring elements. In our experiments, we use a bank of eight distinct 3×3 structuring elements, each designed to detect pixel endpoints of connected foreground components in the fundamental directions: horizontal (right/left), vertical (up/down), and the two diagonals (top-left, top-right, bottom-left, bottom-right). The final set of endpoints is obtained by taking the union of all pixels detected by this operation.

These endpoints serve as the initial points for recovering the individual curves. For each skeleton curve, two endpoints are found: integration starting from one endpoint yields the full trajectory following the orientation of the vector field, while integration from the opposite endpoint produces no trajectory. Figure 2 illustrates this initialization procedure and shows the selected initial points for this experiment. Figure 3 presents another experiment in the same setting, showing that the algorithm is able to separate filaments that are in the same blur pattern.

Building on the vector field deconvolution framework, we now focus on curve reconstruction in fluorescence microscopy, aiming to recover filament structures from degraded image observations.

5.2 Application in Imaging

In many applications, we observe scalar discrete measurements, i.e., pixelated intensity images. In the context of curve reconstruction, the goal is to recover the intrinsic curves hidden within these observed images.

For instance, in fluorescence microscopy, the observed image is degraded due to light diffraction, an inevitable phenomenon in any optical microscope, as well as due to inherent noise in the imaging system. Diffraction can be modeled as a convolution of the ground-

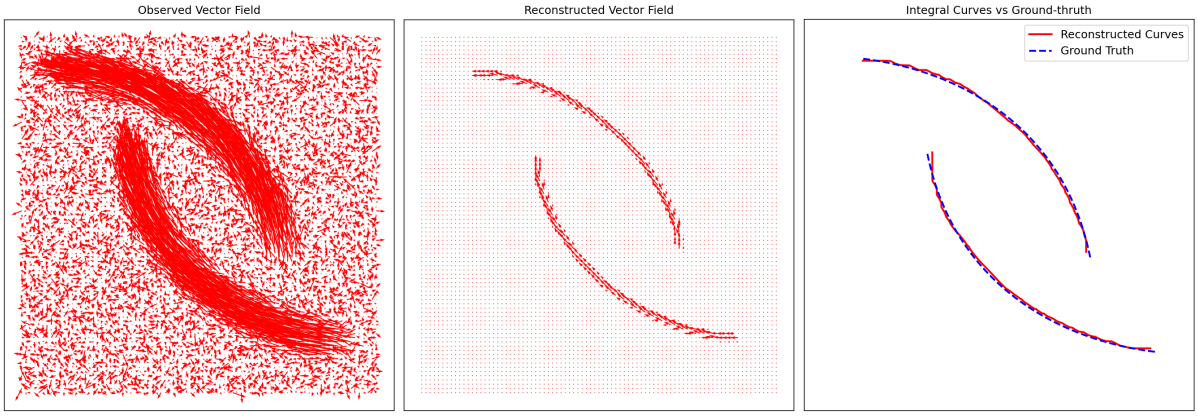

Figure 1: From left to right: observed vector fields, reconstructed fields obtained with the $\mathrm{CROC}_{\mathrm{R}}$ functional, and the reconstructed integral curves (in red) overlaid with the ground truth curves (in blue).

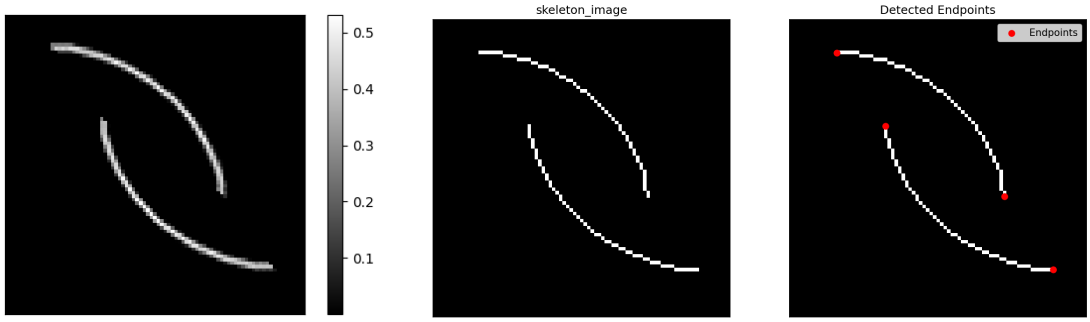

Figure 2: From left to right: the magnitude image of the reconstructed vector field, the computed skeleton, and the skeleton with the selected endpoints used as initialization points for the integral curves.

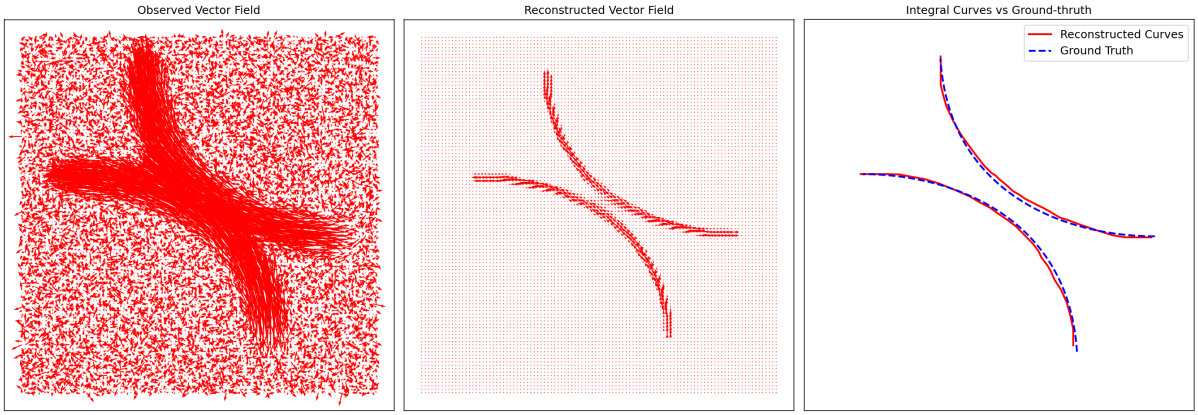

Figure 3: From left to right: observed vector fields, reconstructed fields obtained with the $\mathrm{CROC}_{\mathrm{R}}$ functional, and the reconstructed integral curves (in red) overlaid with the ground truth curves (in blue).

truth structures with the microscope's point spread function (PSF), which is commonly modeled by a Gaussian function and the noise is often assumed to be additive Gaussian for simplicity. Consequently, when imaging curve-like structures, instead of directly observing one-dimensional objects, we obtain blurred regions where the intensity gradually decreases as one moves away from the curve of interest plus a noise, as we can see in Figure 4 a).

In the following, we first describe how the curves and blurry regions are modeled, and then present the process for recover the original curves.

Let $\gamma : [0,1] \to \mathcal{X}$ be a simple parameterized curve with support $\Gamma = \gamma([0,1])$. The blurred curve in the observed image can be modeled as the convolution of the support Γ of the curve γ with the PSF h:

$$\int_0^1 h(\gamma(t) - x)\, \|\dot{\gamma}(t)\|\, \mathrm{d}t, \quad \forall x \in \mathcal{X}, \tag{6}$$

In practice, the curve γ is discretized as a polygonal line defined by its vertices $\{\gamma(t_j)\}_{j=0}^n$, with $t_0 = 0$ and $t_n = 1$. For an image O containing a single curve γ, the intensity O_i at each pixel P_i is approximated as

$$O_i = \sum_{j=0}^{n-1} \|\gamma(t_{j+1}) - \gamma(t_j)\|\, h\Big(\frac{\gamma(t_{j+1}) + \gamma(t_j)}{2} - c_i\Big) + \eta_i, \tag{7}$$

where c_i is the center of the pixel P_i and η_i represents a sample of additive Gaussian noise.

For images containing multiple blurred curves $\{\gamma_k\}_{k=1}^K$ with amplitudes $\{a_k\}_{k=1}^K$, the intensity of each pixel is the weighted sum of the contributions from each curve:

$$O_i = \sum_{k=1}^{K} a_k\, O_i^k, \tag{8}$$

where O_i^k is computed using the same formula as above in (7) for the curve γ_k.

Reconstruction using the $\mathrm{CROC_R}$ functional

To perform the reconstruction using the $\mathrm{CROC_R}$ functional as above, we first have to define a vectorial observation y from the observed intensity O. A straightforward idea is to derive from the observed scalar image O, a vector quantity that allows recovering the velocity vector field associated with the curves hidden in the image.

Since a velocity field involves derivatives, we first consider a data term based on the gradient of the observed image. Because the gradient is orthogonal to the level curves of a function, we define y as the field orthogonal to the image gradient, so that it aligns with the direction of the curves to be recovered. The resulting functional therefore takes the same form as in equation (4), with $(y_1, y_2) = \nabla^\perp O$, where O denotes the observed image.

As illustrated in Figure 4, with this choice, the reconstructed field corresponds to closed contours delineating the blurred regions rather than the actual velocity fields of

the underlying curves. This behavior arises because the orthogonal of the gradient does not accurately represent the blurred and noisy velocity field of the curves: in the discrete gradient of such an image, the values are near zero along the curves of interest and increase when moving away from the blurred regions.

Although the functional itself is well-suited for the deconvolution of vector fields, as shown in the previous subsection, the challenge for image-based observations lies in correctly deriving an observed vector field that represents the underlying blurred velocity field.

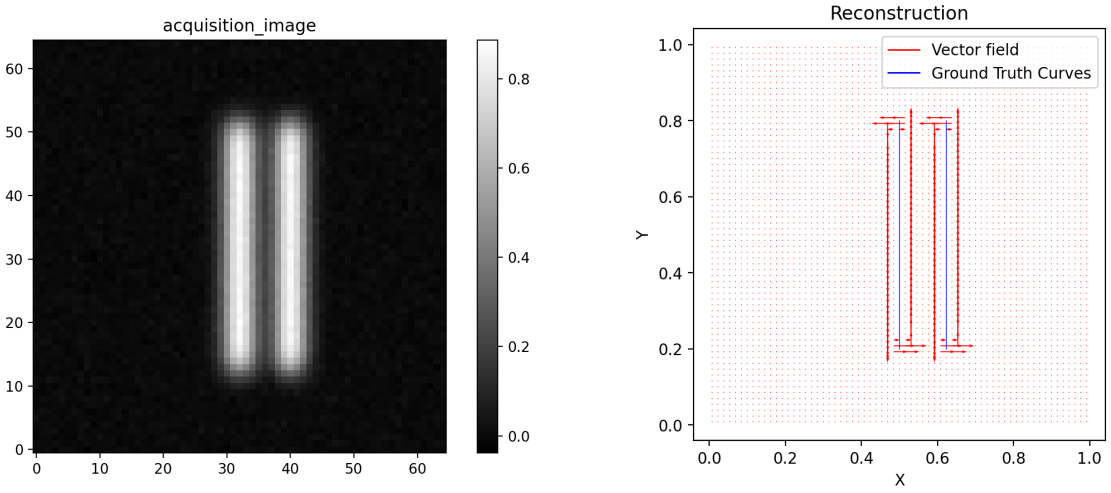

(a) Simulated observed scalar image.

(b) Reconstructed vector field

Figure 4: Simulation results obtained with the $\mathrm{CROC}_{\mathrm{R}}$ functional, using the vector observation modeled as the field orthogonal to the image gradient. (a) Observed image. (b) Reconstructed vector field (red) and ground-truth curve (blue).

A Proposed Functional for Scalar Image Observations

Extracting appropriate vector information from an observed image being challenging, we propose a new data-term model defined directly from the observed scalar image. The new functional is given by

$$\underset{m\in\mathcal{V}(\mathcal{X})}{\arg\min}\, \mathrm{T}_\lambda(m) \overset{\text{def.}}{=} \frac{1}{2}\left\|O - |m| * h\right\|_{\mathcal{H}}^2 + \lambda \left\|m\right\|_{\mathcal{V}(\mathcal{X})}, \tag{9}$$

where $|m|$ is the total variation measure of the vector measure m.
The corresponding functional in the relaxed space $\mathcal{W}$ reads

$$\underset{f\,dx\in\mathcal{W}(\mathcal{X})}{\arg\min}\, D_\lambda(f) \overset{\text{def.}}{=} \frac{1}{2}\left\|O - |f| * h\right\|_{\mathcal{H}}^2 + \lambda \left\|f\right\|_{L^1(\mathcal{X},\mathbb{R}^2)} + \lambda \left\|\mathrm{div}(f)\right\|_{L^1(\mathcal{X},\mathbb{R})}, \tag{10}$$

since a measure $m = f\,dx$, its total variation is given for any Borel set A by

$$|m|(A) = \int_A |f(x)|\,dx, \quad \text{where } |f(x)| = |f_1(x)| + |f_2(x)|, \quad \forall x \in \mathcal{X}.$$

Although this functional is no longer linear or convex, unlike the original $\mathrm{CROC}_{\mathrm{R}}$, the simulation results presented in Figures 5, 6, and 7 demonstrate its potential and promising performance in handling blurred and noisy scalar images containing curve structures. In particular, the proposed algorithm avoids the support extraction step required in the CSFW algorithm, which is a very challenging problem.

The implementation code associated with this work is available at the following repository: https://gitlab.inria.fr/atsafack/implementation-of-croc_relaxed-functional-on-w.

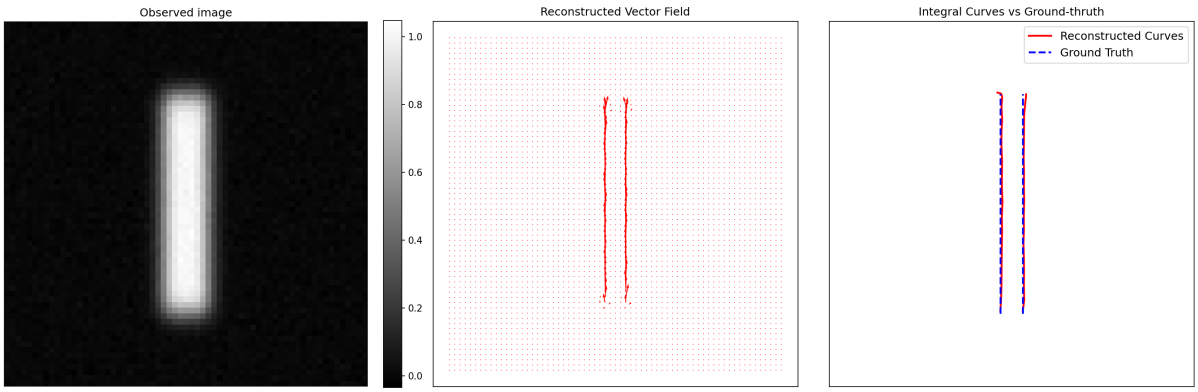

Figure 5: Experiment results for two overlapping curves in the blur region. From left to right: the observed blurry and noisy image, the reconstructed vector field, and the computed integral curves (in red) overlaid with the ground truth (in blue).

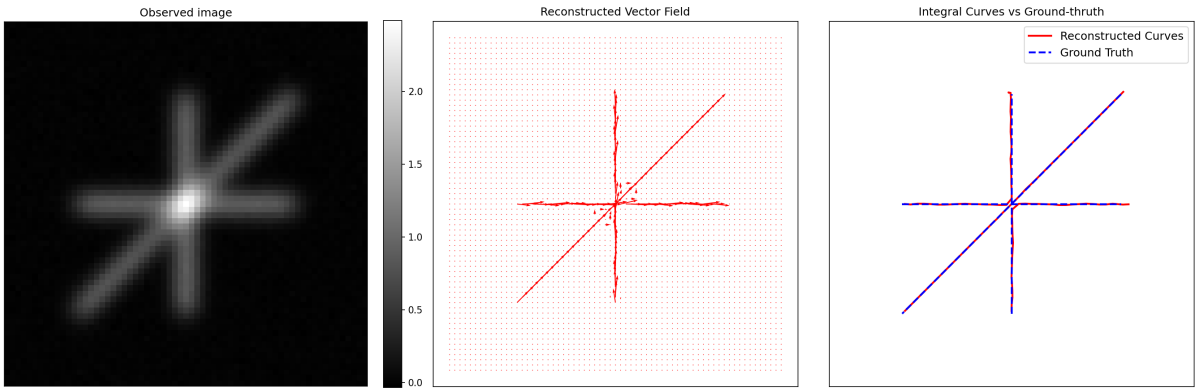

Figure 6: Experiment results for crossing curves. From left to right: the observed blurry and noisy image, the reconstructed vector field, and the computed integral curves (in red) overlaid with the ground truth (in blue).

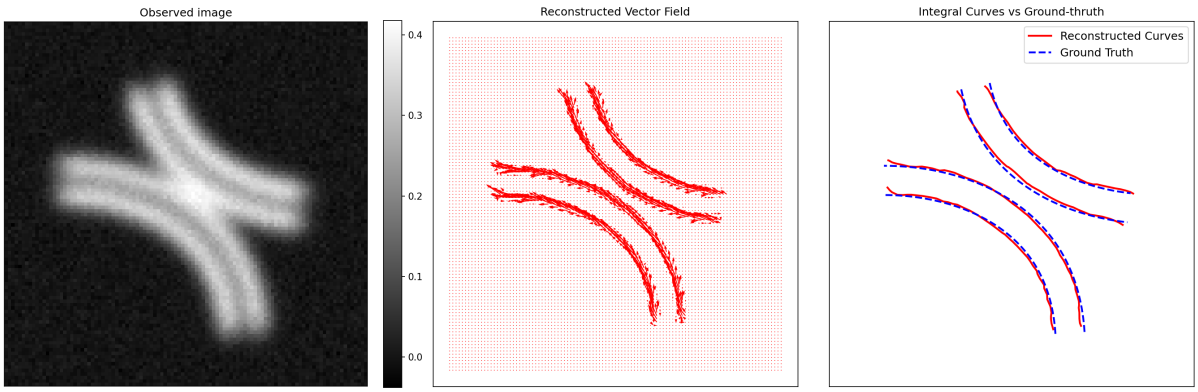

Figure 7: Experiment results for four curves. From left to right: the observed blurry and noisy image, the reconstructed vector field, and the computed integral curves (in red) overlaid with the ground truth (in blue).

Conclusion

This work proposes a new approach for optimizing the CROC functional, allowing the use of classical optimization algorithms for numerical implementation. We introduced the space $\mathcal{W}(\mathcal{X})$, which is dense in $\mathcal{V}(\mathcal{X})$ for the local weak-* topology. The associated functional, $\mathrm{CROC}_{\mathrm{R}}$, is well suited for vector field deconvolution and is convex. We prove that any minimizing sequence of this functional $\mathrm{CROC}_{\mathrm{R}}$ converges to a solution of the original CROC functional.

In the context of imaging, the main challenge is to define a vector-valued quantity that accurately represents the curves. Using the orthogonal of the image gradient to define an observed vector field captures the contours of blurred regions rather than the curves themselves. Due to the challenge, we propose a new functional with a scalar data term directly based on the observed image. This new functional shows significant potential, and further theoretical and numerical investigations will be the focus of an upcoming paper.

A. Proofs of density results

We begin with the following lemma, which provides an exhaustion of the open set by compact subsets.

Lemma A.1. *Let $\Omega \subset \mathbb{R}^2$ be an open set. For each $\varepsilon > 0$, define*

$$K_\varepsilon := \left\{ x \in \mathbb{R}^2 \;\middle|\; d(x, \Omega^c) \geq 2\varepsilon \text{ and } \|x\| \leq \frac{1}{\varepsilon} \right\}.$$

Then K_ε is compact, $K_\varepsilon \subset \Omega$, and $\Omega = \bigcup_{\varepsilon>0} K_\varepsilon$.

For $\varepsilon > 0$, we define

$$g_\varepsilon := \mathbb{1}_{K_{2\varepsilon/3}} * \rho_{2\varepsilon/3}.$$

Then $g_\varepsilon \in \mathcal{C}^\infty(\mathbb{R}^2, \mathbb{R})$, and

$$\operatorname{spt}(g_\varepsilon) \subset K_{2\varepsilon/3} + B\left(0, \frac{2\varepsilon}{3}\right) \subset \Omega.$$

Since $K_{2\varepsilon/3}$ is compact, it follows that $g_\varepsilon \in \mathcal{C}_c^\infty(\Omega, \mathbb{R})$. Moreover, for each $\varepsilon > 0$,

$$0 \leq g_\varepsilon \leq 1 \qquad \text{and} \qquad g_\varepsilon \equiv 1 \text{ on } K_\varepsilon.$$

Now define

$$f_\varepsilon := g_\varepsilon \, (\rho_{\varepsilon/3} * m).$$

Then $f_\varepsilon \in \mathcal{C}_c^\infty(\Omega, \mathbb{R}^2)$. In particular, $f_\varepsilon \in L^1(\Omega)^2$. Moreover, since $\operatorname{div}(f_\varepsilon) \in \mathcal{C}_c^\infty(\Omega, \mathbb{R})$, we also have $\operatorname{div}(f_\varepsilon) \in L^1(\Omega)$. One then checks that

$$f_\varepsilon \, dx \overset{*}{\rightharpoonup} m \quad \text{in } \mathcal{M}(\Omega)^2, \qquad \operatorname{div}(f_\varepsilon) \overset{*}{\rightharpoonup} \operatorname{div}(m) \quad \text{locally in } \mathcal{M}(\Omega).$$

Therefore, $f_\varepsilon \, dx$ converges to m in the local weak-* topology of $\mathcal{V}(\Omega)$, which proves Proposition 3.3 and Remark 3.4.

B. Proof of Theorem 4.3

We will consider a given kernel ϕ and its associated $\varphi \in C_0(\mathcal{X}, \mathbb{R})^2$, as an *acquisition kernel* for the CROC problem.

Since $\mathcal{W}(\mathcal{X}) \subset \mathcal{V}(\mathcal{X})$, it follows that

$$\inf_{m \in \mathcal{V}(\mathcal{X})} T_\lambda(m) \leq \inf_{m \in \mathcal{W}(\mathcal{X})} D_\lambda(m). \tag{11}$$

To establish equality, it remains to prove the reverse inequality.

Let $\overline{m} \in \mathcal{V}(\mathcal{X})$ be a minimizer of the CROC functional that can be written as a finite linear combination of measures supported on curves:

$$\overline{m} = \sum_{i=1}^{N} a_i \, \mu_{\gamma_i},$$

where each $\gamma_i : [0,1] \to \mathcal{X}$ is a parametrized curve whose image is contained in $\mathcal{X}$. The existence of such a minimizer is established in [9]; see also the Introduction. Since $\mathcal{X} \subset \mathbb{R}^2$, each γ_i can also be regarded as a curve in $\mathbb{R}^2$. Hence, each μ_{γ_i} defines a vector-valued finite Radon measure on $\mathbb{R}^2$. and hence each μ_{γ_i} defines a vector-valued finite Radon measure on $\mathbb{R}^2$. Moreover, in the sense of distributions on $\mathbb{R}^2$,

$$\operatorname{div}(\mu_{\gamma_i}) = \delta_{\gamma_i(0)} - \delta_{\gamma_i(1)}.$$

Therefore,

$$\operatorname{div}(\overline{m}) = \sum_{i=1}^{N} a_i \big(\delta_{\gamma_i(0)} - \delta_{\gamma_i(1)}\big)$$

is a finite Radon measure on $\mathbb{R}^2$, and thus $\overline{m} \in \mathcal{V}(\mathbb{R}^2)$.

1. *Step 1: Mollification of $\overline{m}$.* We consider a family of standard mollifiers $(\rho_\varepsilon)_{\varepsilon>0}$, as defined in Definition 2.10. Let

$$\bar{f}_\varepsilon := \overline{m} * \rho_\varepsilon \quad \text{for all } \varepsilon > 0.$$

Since $\overline{m} \in \mathcal{M}(\mathbb{R}^2)^2$, the convolution is well defined on $\mathbb{R}^2$, $\bar{f}_\varepsilon \in C^\infty(\mathbb{R}^2;\mathbb{R}^2)$, and

$$\bar{f}_\varepsilon \,\mathrm{d}x \overset{*}{\rightharpoonup} \overline{m} \ \text{ in } \mathcal{M}(\mathbb{R}^2)^2 \quad \text{as } \varepsilon \to 0.$$

Moreover,

$$|\bar{f}_\varepsilon \,\mathrm{d}x|(\mathbb{R}^2) \le |\overline{m}|(\mathbb{R}^2) \qquad \text{for all } \varepsilon > 0.$$

Since $\operatorname{supp}(\overline{m}) \subset \mathcal{X}$, it follows in particular that

$$|\bar{f}_\varepsilon \,\mathrm{d}x|(\mathcal{X}) \le |\overline{m}|(\mathcal{X}) \qquad \text{for all } \varepsilon > 0. \tag{12}$$

Also note that $\operatorname{div}(\bar{f}_\varepsilon) = \operatorname{div}(\overline{m}) * \rho_\varepsilon$, $\operatorname{div}(\bar{f}_\varepsilon\, dx) \overset{*}{\rightharpoonup} \operatorname{div}(\overline{m})$ in $\mathcal{M}(\mathbb{R}^2)$ as $\varepsilon \to 0$, and

$$\big|\operatorname{div}(\bar{f}_\epsilon \,\mathrm{d}x)\big|\,(\mathcal{X}) \le |\operatorname{div}(\overline{m})|(\mathcal{X}), \qquad \text{for all } \epsilon > 0. \tag{13}$$

To simplify notation in the next steps, we set $\overline{m}_\varepsilon := \bar{f}_\varepsilon\, dx$, and denote by $\overline{m}_\varepsilon|_{\mathcal{X}}$ the restriction of $\overline{m}_\varepsilon$ to $\mathcal{X}$.

2. *Step 2: Convergence of $T_\lambda(\overline{m}_\epsilon|_{\mathcal{X}})$ to $T_\lambda(\overline{m})$.*

Since $\overline{m}_\epsilon \overset{*}{\rightharpoonup} \overline{m}$ on $\mathbb{R}^2$, it follows that

$$\liminf_{\epsilon\to 0} |\overline{m}_\epsilon|(\mathcal{X}) \ge |\overline{m}|(\mathcal{X}),$$

due to the lower semicontinuity of the total variation norm with respect to the weak-* convergence on every open set. Consequently, we have

$$|\overline{m}|(\mathcal{X}) \le \liminf_{\epsilon\to 0} |\overline{m}_\epsilon|(\mathcal{X}) \le \limsup_{\epsilon\to 0} |\overline{m}_\epsilon|(\mathcal{X}) \le |\overline{m}|(\mathcal{X}),$$

where the last inequality follows from equation (12). Therefore, we conclude that

$$\lim_{\epsilon\to 0} |\overline{m}_\epsilon|(\mathcal{X}) = |\overline{m}|(\mathcal{X}). \tag{14}$$

By applying the same argument and using equation (13), we also deduce that

$$\lim_{\epsilon\to 0} |\mathrm{div}(\overline{m}_\epsilon)|(\mathcal{X}) = |\mathrm{div}(\overline{m})|(\mathcal{X}). \tag{15}$$

Remark that

$$\|y - \Phi(\overline{m}_\epsilon|_{\mathcal{X}})\|^2_{L^2(\mathcal{X})} = \|y\|^2_{L^2(\mathcal{X})} - 2\langle y, \Phi(\overline{m}_\epsilon|_{\mathcal{X}})\rangle_{L^2(\mathcal{X})} + \|\Phi(\overline{m}_\epsilon|_{\mathcal{X}})\|^2_{L^2(\mathcal{X})}\,. \tag{16}$$

Since $\overline{m}_\varepsilon \overset{*}{\rightharpoonup} \overline{m}$ in $\mathcal{M}(\mathbb{R}^2)^2$, the restriction $\overline{m}_\varepsilon|_{\mathcal{X}}$ locally weak-* converges to $\overline{m}|_{\mathcal{X}} = \overline{m}$ in $\mathcal{M}(\mathcal{X})^2$, due to the inclusion $C_c(\mathcal{X};\mathbb{R})^2 \subset C_c(\mathbb{R}^2;\mathbb{R})^2$. Furthermore, the uniform bound

$$\sup_{\varepsilon>0} |\overline{m}_\varepsilon|_{\mathcal{X}}|(\mathcal{X}) = \sup_{\varepsilon>0} |\overline{m}_\varepsilon|(\mathcal{X}) \leq |\overline{m}|(\mathcal{X}) < \infty$$

ensures the weak-* convergence of the restricted measures in $\mathcal{M}(\mathcal{X})^2$, by Proposition 2.9.

This implies

$$\langle y, \Phi(\overline{m}_\epsilon|_{\mathcal{X}})\rangle_{L^2(\mathcal{X})} \xrightarrow{\epsilon\to 0} \langle y, \Phi(\overline{m})\rangle_{L^2(\mathcal{X})}. \tag{17}$$

since Φ is weak*-to-weak continuous from $\mathcal{M}(\mathcal{X})^2$ to $L^2(\mathcal{X})$.

Furthermore,

$$\|\Phi(\overline{m}_\epsilon|_{\mathcal{X}})\|^2_{L^2(\mathcal{X})} = \int_{\mathcal{X}} \left(\Phi(\overline{m}_\epsilon|_{\mathcal{X}})(x)\right)^2 \mathrm{d}x = \int_{\mathcal{X}} |\langle \overline{m}_\epsilon|_{\mathcal{X}}, \varphi(\cdot - x)\rangle|^2 \ \mathrm{d}x. \tag{18}$$

Since $\forall x \in \mathcal{X},\ \varphi(\cdot - x) \in \mathcal{C}_0(\mathcal{X}, \mathbb{R}^2)$, and $\overline{m}_\epsilon|_{\mathcal{X}} \overset{*}{\rightharpoonup} \overline{m}$ in $\mathcal{M}(\mathcal{X})^2$, then

$$\forall x \in \mathcal{X},\ \langle \overline{m}_\epsilon|_{\mathcal{X}}, \varphi(\cdot - x)\rangle \xrightarrow{\epsilon\to 0} \langle \overline{m}, \varphi(\cdot - x)\rangle\,. \tag{19}$$

Moreover, for all $x \in \mathcal{X}$,

$$\begin{aligned} |\langle \overline{m}_\epsilon|_{\mathcal{X}}, \varphi(\cdot - x)\rangle| &= \left|\int_{\mathcal{X}} \varphi(y - x)\ \mathrm{d}\overline{m}_\epsilon(y)\right| \\ &\leq \|\varphi\|_\infty\ |\overline{m}_\epsilon|(\mathcal{X}) \\ &\leq \|\varphi\|_\infty |\overline{m}|(\mathcal{X}). \end{aligned} \tag{20}$$

Due to equation (19) and equation (20), we can apply the Lebesgue Dominated Convergence Theorem to the integral in equation (18), to get:

$$\lim_{\epsilon\to 0} \int_{\mathcal{X}} \langle \overline{m}_\epsilon|_{\mathcal{X}}, \varphi(\cdot - x)\rangle^2 \,\mathrm{d}x = \int_{\mathcal{X}} \langle \overline{m}, \varphi(\cdot - x)\rangle^2 \,\mathrm{d}x, \tag{21}$$

meaning that

$$\|\Phi(\overline{m}_\epsilon|_{\mathcal{X}})\|^2_{L^2(\mathcal{X})} \xrightarrow{\epsilon\to 0} \|\Phi(\overline{m})\|^2_{L^2(\mathcal{X})}. \tag{22}$$

From the equations (16), (17) and (22), we get

$$\frac{1}{2}\left\|y-\Phi(\overline{m}_\epsilon)\right\|^2_{L^2(\mathcal{X})} \xrightarrow{\epsilon\to 0} \frac{1}{2}\left\|y-\Phi(\overline{m})\right\|^2_{L^2(\mathcal{X})}. \tag{23}$$

Hence, from equations (12) and (13), we conclude that:

$$\mathrm{T}_\lambda(\overline{m}_\epsilon|_{\mathcal{X}}) = \frac{1}{2}\left\|y-\Phi(\overline{m}_\epsilon|_{\mathcal{X}})\right\|^2_{L^2(\mathcal{X})} + \lambda\ |\overline{m}_\epsilon|(\mathcal{X}) + \lambda\ |div(\overline{m}_\epsilon)|(\mathcal{X})$$

converges as $\epsilon \to 0$ to

$$\mathrm{T}_\lambda(\overline{m}) = \frac{1}{2}\left\|y-\Phi(\overline{m})\right\|^2_{L^2(\mathcal{X})} + \lambda\ |\overline{m}|(\mathcal{X}) + \lambda\ |div(\overline{m})|(\mathcal{X}).$$

3. *Step 3: Inequality between infima.*

   By the definition of convergence, for any $\delta > 0$, there exists $\epsilon_0 > 0$ such that for all $\epsilon \in (0, \epsilon_0)$,

   $$\mathrm{T}_\lambda(\overline{m}_\epsilon|_{\mathcal{X}}) \leq \mathrm{T}_\lambda(\overline{m}) + \delta.$$

   Since $\overline{m}_\epsilon|_{\mathcal{X}} \in \mathcal{W}(\mathcal{X})$, we deduce that for any $\delta > 0$, there exists $\epsilon_0 > 0$ such that for all $\epsilon \in (0, \epsilon_0)$, the following holds:

   $$\inf_{m\in\mathcal{W}(\mathcal{X})} \mathrm{T}_\lambda(m) \leq \mathrm{T}_\lambda(\overline{m}) + \delta = \inf_{m\in\mathcal{V}(\mathcal{X})} \mathrm{T}_\lambda(m) + \delta.$$

   By letting $\delta \to 0$, we obtain:

   $$\inf_{m\in\mathcal{W}(\mathcal{X})} D_\lambda(m) \leq \inf_{m\in\mathcal{V}(\mathcal{X})} T_\lambda(m),$$

   which completes the proof of Theorem 4.3.

C. Acknowledgments

The work of T.A.D has been supported by the French government, through the France 2030 investment plan managed by the Agence Nationale de la Recherche, as part of the Université Côte d'Azur's Initiative of Excellence, reference ANR-15-IDEX-01 and of the "UCA DS4H" project, reference ANR-17-EURE-0004. The work of LBF has been supported by the French government, through the 3IA Côte d'Azur Investments in the Future project managed by the National Research Agency (ANR) with the reference number ANR-19-P3IA-0002.

References

[1] Luigi Ambrosio, Nicola Fusco & Diego Pallara. *Functions of bounded variation and free discontinuity problems*. Oxford university press, 2000.

[2] Paolo Bonicatto & Nikolay A. Gusev. 'On the structure of divergence-free measures on $\mathbb{R}^2$'. In: *Advances in Calculus of Variations* 15.4 (2022), pp. 879–911. URL: https://doi.org/10.1515/acv-2020-0066.

[3] Kristian Bredies & Hanna Katriina Pikkarainen. 'Inverse problems in spaces of measures'. In: *ESAIM: Control, Optimisation and Calculus of Variations* 19.1 (2013), pp. 190–218.

[4] H Brezis. *Functional Analysis, Sobolev Spaces and Partial Differential Equations*. 2011.

[5] Antonin Chambolle. 'An algorithm for total variation minimization and applications'. In: *Journal of Mathematical imaging and vision* 20.1 (2004), pp. 89–97.

[6] Quentin Denoyelle et al. *The Sliding Frank-Wolfe Algorithm and its Application to Super-Resolution Microscopy*. 2018. arXiv: 1811.06416 [math.NA]. URL: https://arxiv.org/abs/1811.06416.

[7] R.C. Gonzalez, R.C. Woods & R.E. Woods. *Digital Image Processing*. Addison-Wesley world student series. Addison-Wesley, 1992. ISBN: 9780201508031. URL: https://books.google.fr/books?id=CfQeAQAAIAAJ.

[8] Bastien Laville, Laure Blanc-Féraud & Gilles Aubert. 'A Γ-Convergence Result and An Off-the-Grid Charge Algorithm for Curve Reconstruction in Inverse Problems'. In: *Journal of Mathematical Imaging and Vision* 66.4 (2024), pp. 572–583. ISSN: 1573-7683. DOI: 10.1007/s10851-024-01190-1. URL: https://doi.org/10.1007/s10851-024-01190-1.

[9] Bastien Laville, Laure Blanc-Féraud & Gilles Aubert. 'Off-the-Grid Curve Reconstruction through Divergence Regularization: An Extreme Point Result'. In: *SIAM Journal on Imaging Sciences* 16.2 (2023), pp. 867–885. URL: https://doi.org/10.1137/22M1494373.

[10] Dong C Liu & Jorge Nocedal. 'On the limited memory BFGS method for large scale optimization'. In: *Mathematical programming* 45.1 (1989), pp. 503–528.

[11] Halsey Royden & Patrick Michael Fitzpatrick. *Real analysis*. China Machine Press, 2010.

[12] Miroslav Šilhavỳ. 'The divergence theorem for divergence measure vectorfields on sets with fractal boundaries'. In: *Mathematics and mechanics of solids* 14.5 (2009), pp. 445–455.

[13] Smirnov. 'Decomposition of solenoidal vector charges into elementary solenoids and the structure of normal one-dimensional currents'. In: *St. Petersburg Mathematical Journal* 5.4 (1994), pp. 841–867.

[14] Pierre Soille. 'Introduction'. In: *Morphological Image Analysis: Principles and Applications*. Berlin, Heidelberg: Springer Berlin Heidelberg, 1999, pp. 1–13. ISBN: 978-3-662-03939-7. DOI: 10.1007/978-3-662-03939-7_1. URL: https://doi.org/10.1007/978-3-662-03939-7_1.